Supplementary data (Figures S1-S25)

Enhanced Cancer Therapy with Cold-Controlled Drug Release and Photothermal Warming Enabled with One Nanoplatform

Hai Wang[1,2,3], Pranay Agarwal[2], Yutong Liang[1], Jiangsheng Xu[1,2,3], Gang Zhao[4], Katherine H.R. Tkaczuk[5] , Xiongbin Lu[6], Xiaoming He[1,2,3,5,7]*

[1]Fischell Department of Bioengineering, University of Maryland, College Park, MD 20742, USA

[2]Department of Biomedical Engineering, The Ohio State University, Columbus, OH 43210, USA

[3]Comprehensive Cancer Center, The Ohio State University, Columbus, OH 43210, USA

[4]Center for Biomedical Engineering, Department of Electronic Science and Technology, University of Science and Technology of China, Hefei, Anhui 230027, China

[5]Marlene and Stewart Greenebaum Comprehensive Cancer Center, University of Maryland, Baltimore, MD 21201, USA

[6] Department of Medical and Molecular Genetics and Melvin and Bren Simon Cancer Center, Indiana University School of Medicine, Indianapolis, IN 46202, USA

[7]Robert E. Fischell Institute for Biomedical Devices, University of Maryland, College Park, MD 20742, USA

*Correspondence should be addressed to:
X.H.: shawnhe@umd.edu

SUPPLEMENTARY FIGURES

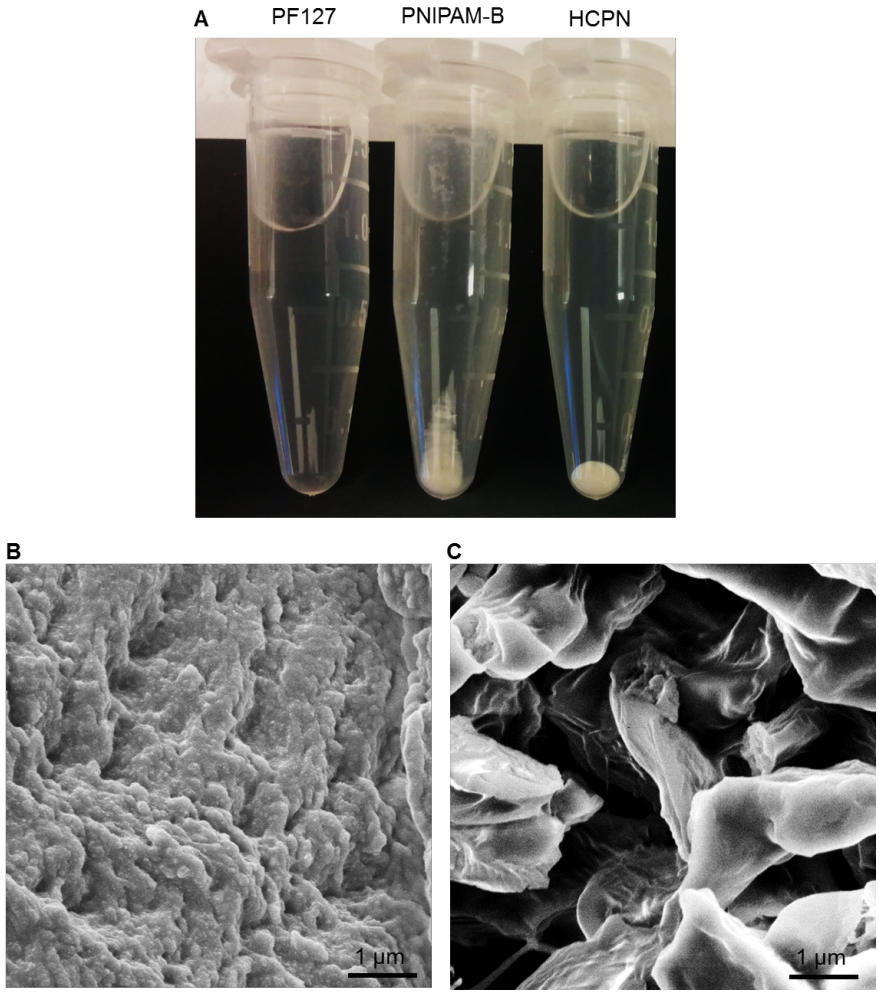

Figure S1. Characterization of nanoparticles prepared with Pluronic F127 (PF127) and PNIPAM-B. (A) A typical picture of the samples obtained after preparing nanoparticles with PF127 alone and PNIPAM-B alone using the double emulsion method, together with HCPN nanoparticles in deionized water. All samples are after centrifugation in 1.5-ml centrifuge tubes. (B) Scanning electron microscopy (SEM) image of the freeze-dried sample obtained by preparing nanoparticles with PF127 alone using the double emulsion method. (C) SEM image of the sample obtained by preparing nanoparticles with PNIPAM-B alone using the double emulsion after centrifugation. The data indicate that nanoparticles cannot be formed with PF127 or PNIPAM-B alone using the double emulsion method.

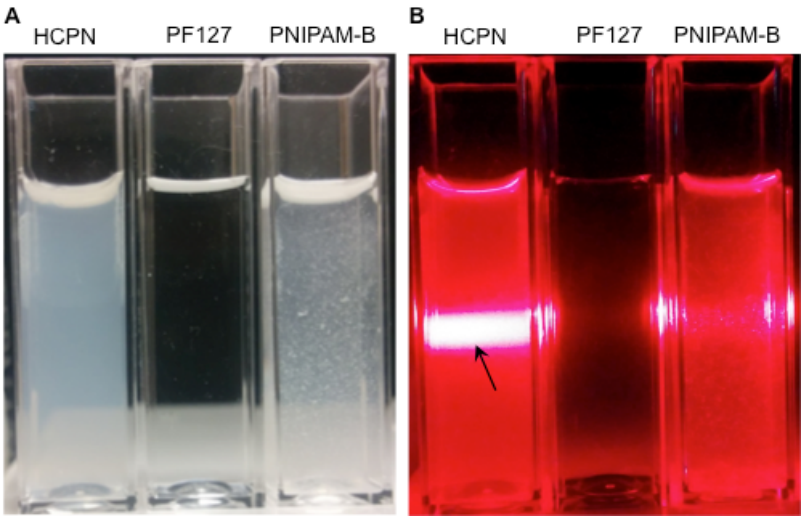

Figure S2. Nanoparticles prepared by combining PF127 and PNIPAM-B together. (A) A typical picture of HCPN nanoparticles in deionized water (2 mg/ml) and the samples obtained after preparing nanoparticles with PF127 alone and PNIPAM-B alone using the double emulsion method. The HCPN nanoparticles can be well dispersed in deionized water, the sample prepared with PF127 alone is transparent, and aggregates are visible in the sample prepared with PNIPAM-B alone. (B) A typical photograph of the aqueous solutions of HCPN nanoparticles and the two samples prepared with PF127 and PNIPAM alone after shining a red laser beam through them in the dark. As a result of the Tyndall effect (i.e., scattering of laser beam by nanoparticles in solution), a light track (indicated by arrow) is visible in the dark in the solution of HCPN nanoparticles while it is not clearly visible in the other two samples. This indicates the HCPN nanoparticles can be stably dispersed in deionized water, and the amount of nanoparticles in the other two samples is negligible.

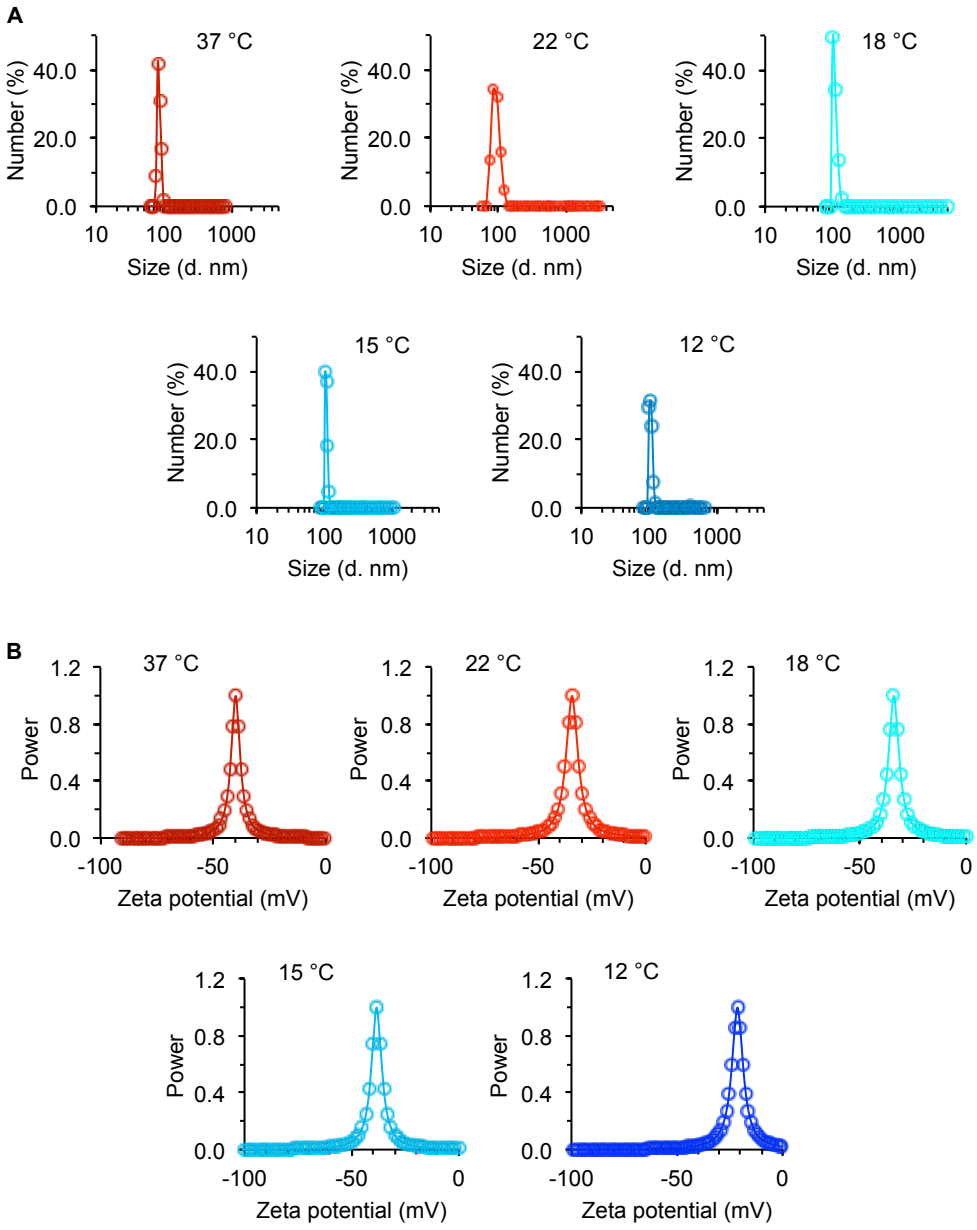

Figure S3. Size distribution and zeta potential of HCPN-CG nanoparticles. The size distribution (A) and zeta potential (B) of HCPN-CG nanoparticles were determined by dynamic light scattering (DLS) at different temperatures. Neither a stable size distribution nor zeta potential could be detected when the temperature is decreased to 10 or 6 °C.

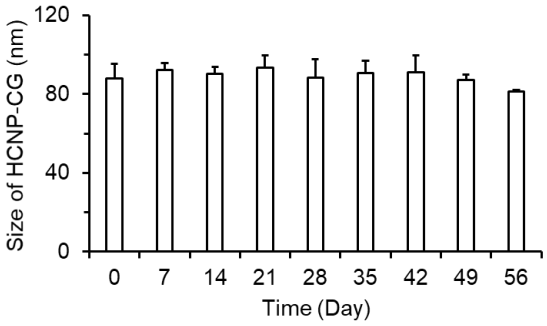

Figure S4. Stability of HCPN-CG nanoparticles. The nanoparticles are stable in aqueous solution at room temperature for at least 56 days. The size of the nanoparticles (2 mg/ml) was determined using DLS. Error bars represent S.D. (n = 3).

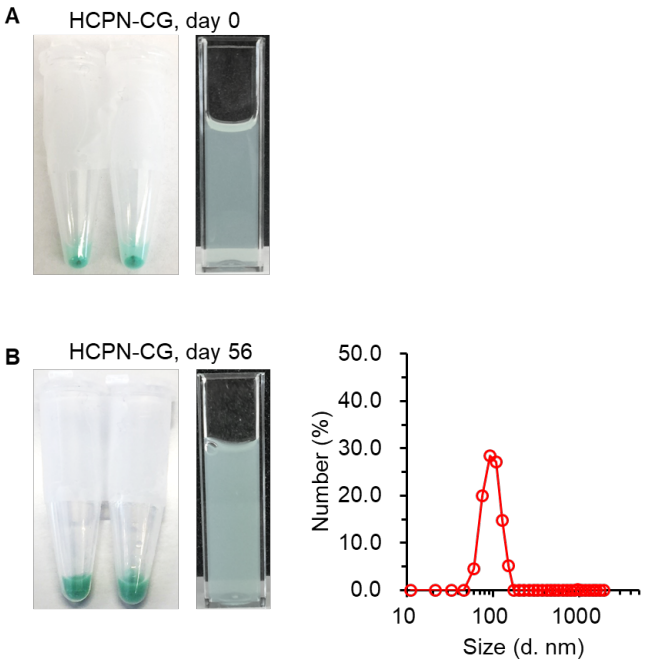

Figure S5. Stability of HCPN-CG nanoparticles at room temperature for 56 days. (A) Photograph of HCPN-CG nanoparticles in the centrifuge tube immediately after centrifugation and removal of nearly all supernatant on day 0 and (B) Photograph of the samples in (A) after storing them at room temperature for 56 days together with the size distribution of the nanoparticles in the samples determined by DLS. The HCPN-CG nanoparticles can be homogenously dispersed in DI water with a narrow size distribution and an average diameter of ~90 nm.

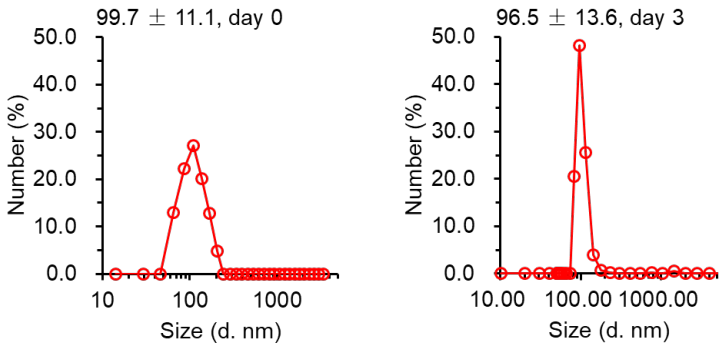

Figure S6. Stability of HCPN-CG nanoparticles in fetal bovine serum (FBS). The size distribution of the HCPN-CG nanoparticles in the FBS was determined by DLS on days 0 and 3, and the data suggest the HCPN-CG nanoparticles are stable under the physiological condition for at least 3 days.

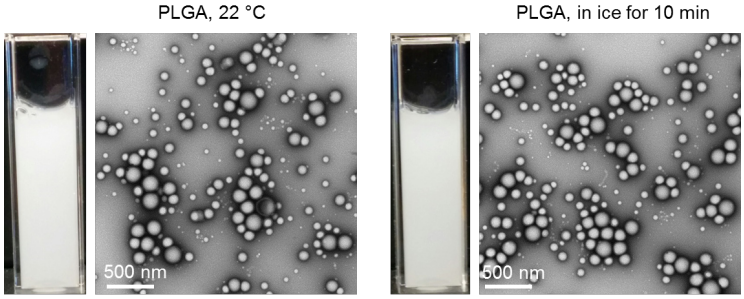

Figure S7. Characterization of nanoparticles prepared by replacing PNIPAM-B with the same amount of PLGA with other conditions being the same. Both the photograph and TEM images show that the PLGA-based nanoparticles are not cold responsive, suggesting the cold-responsive property of HCPN nanoparticles is due to PNIPAM-B.

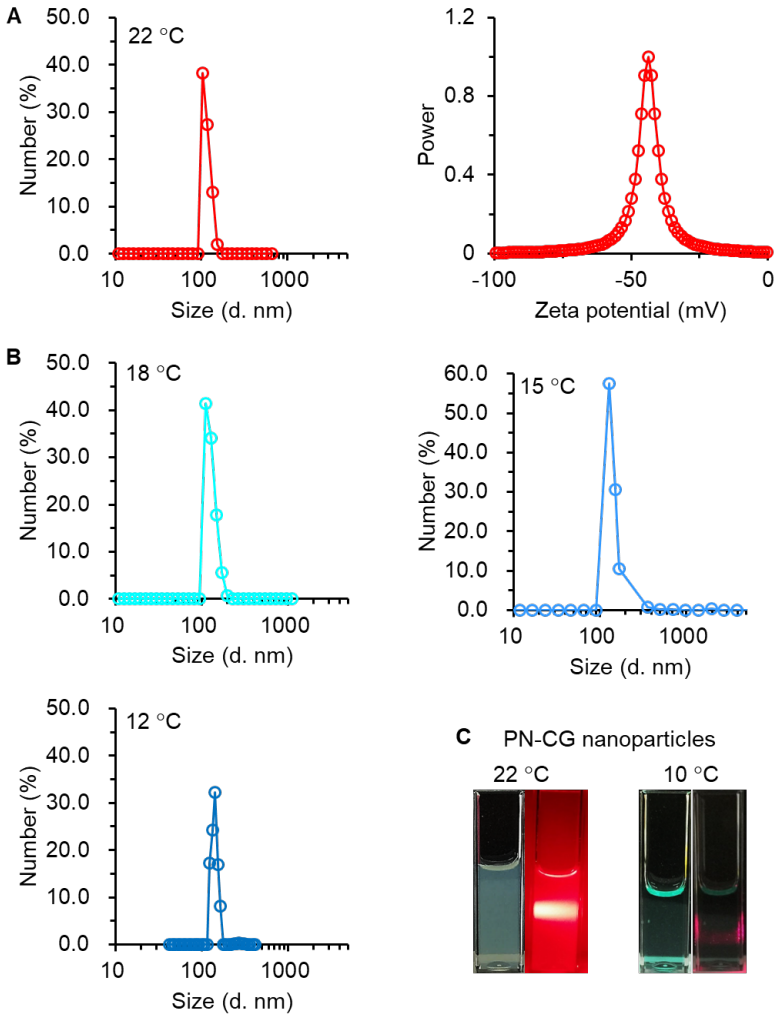

Figure S8. Characterization of the cold-responsiveness of PN-CG nanoparticles. (A) The size distribution of the PN-CG nanoparticles is narrow and their surface is negatively charged. (B) The size distribution of the PN-CG nanoparticles is measureable at 18, 15, and 12 °C, but could not be detected consistently when the temperature is decreased to 10 or 6 °C. (C) Photographs of the aqueous samples of PN-CG nanoparticles at 22 and 10 °C before and after shining a red laser beam through them in the dark. As a result of the Tyndall effect (i.e., scattering of laser beam by nanoparticles in solution), a bright white track of light is visible in the dark in the solutions of PN-CG nanoparticles at 22 °C. However, it is not clearly observable at 10 °C, indicating the PN-CG nanoparticles disassemble upon cooling to 10 °C (or a lower temperature).

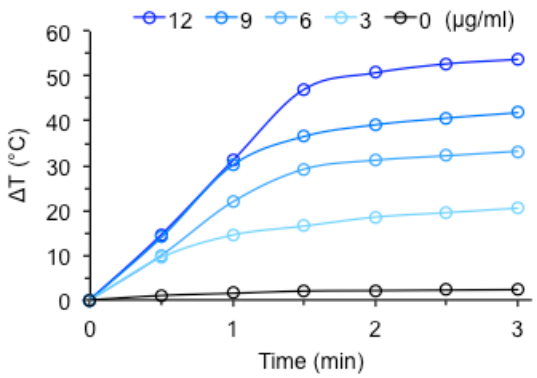

Figure S9. The photothermal effect of HCPN-CG nanoparticles. The irradiation time and ICG concentration dependent increase of temperature in PBS (0 μg/ml) and in the solutions of HCPN-CG nanoparticles in PBS with 3, 6, 9, and 12 μg/ml ICG. The laser irradiation power is 1 W/cm^2.

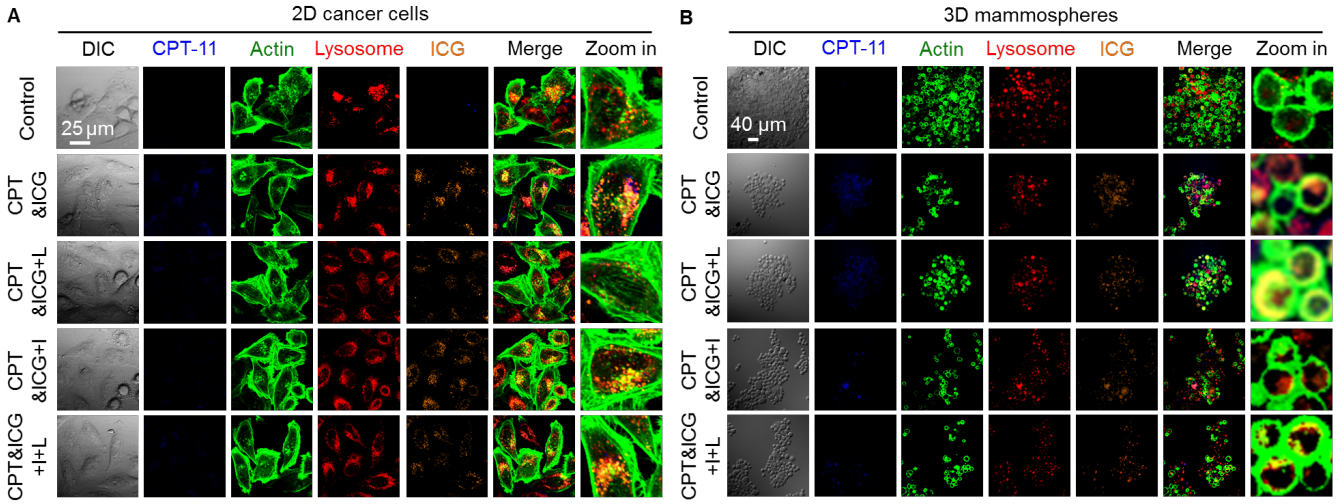

Figure S10. *In vitro* cell uptake of free CPT and ICG. Confocal micrographs of (A) 2D cancer cells and (B) 3D mammosphere cells after incubating with the simple mixture of free CPT&ICG for 3 h at 37 °C, followed by cooling on ice (+I, 5 min), laser irradiation (+L, 1 W/cm^2, 2 min), or both (+I+L). The cell morphology does not change after the different treatments.

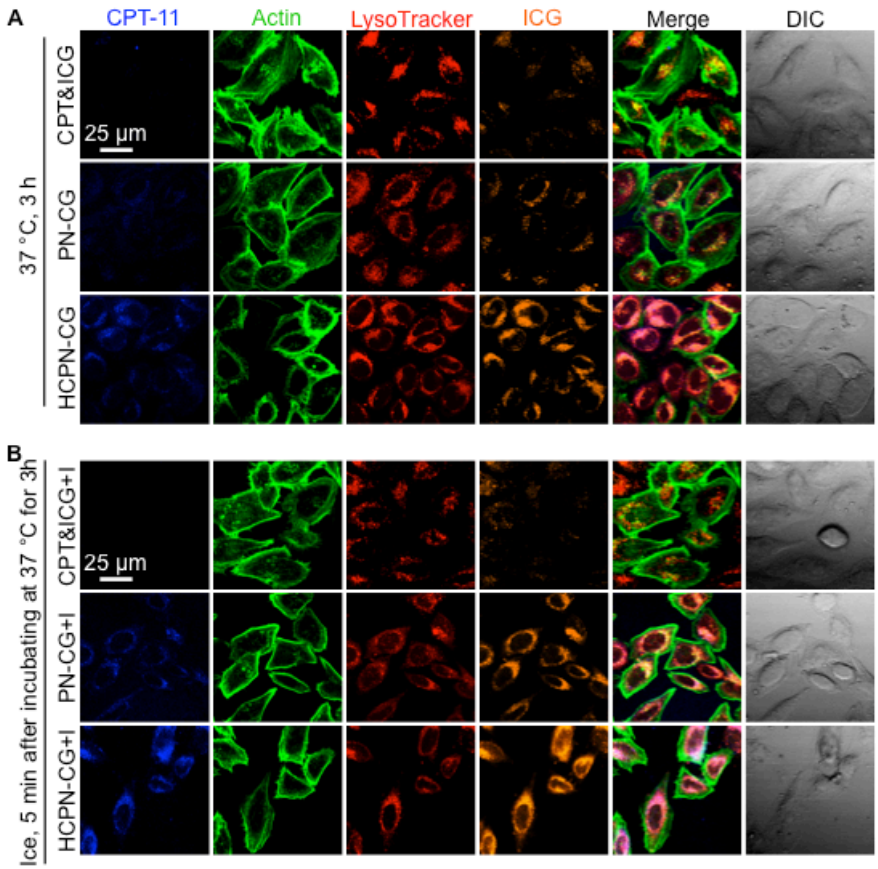

Figure S11. Cold-responsive HCPN-CG nanoparticles for targeted delivery of CPT to MDA-MB-231 cancer cells. (A) Confocal images of MDA-MB-231 cells after incubated with the simple mixture of free CPT&ICG, PN-CG nanoparticles, and HCPN-CG nanoparticles for 3 h at 37 °C and then (B) incubated in ice for 5 min, showing HCPN-CG nanoparticles could be used to improve the delivery of CPT into the cells. The data also show increased fluorescence intensity after ice treatment as a result of the cold-responsive release of CPT from the nanoparticles to reduce quenching of CPT fluorescence in the nanoparticles.

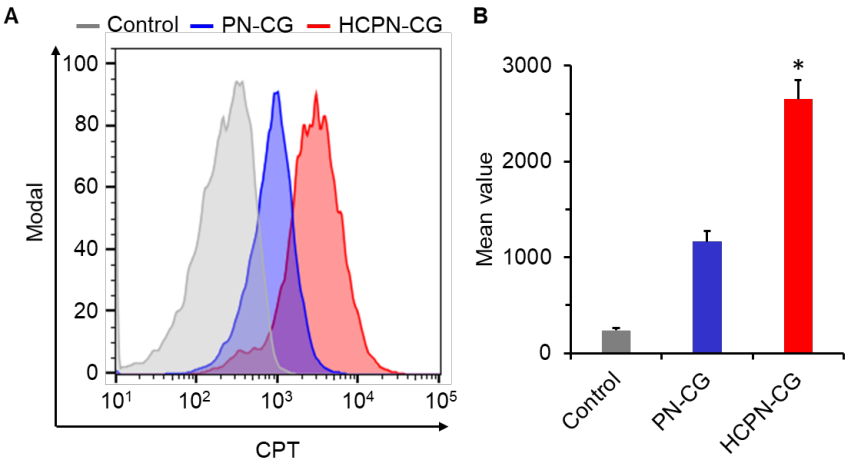

Figure S12. Characterization of the targeting capability of the HCPN-CG nanoparticles with flow cytometry. Typical flow cytometry peaks (A) and mean intensity (B) showing that the HCPN-CG nanoparticles could deliver more CPT into MDA-MB-231 cells than the PN-CG nanoparticles.

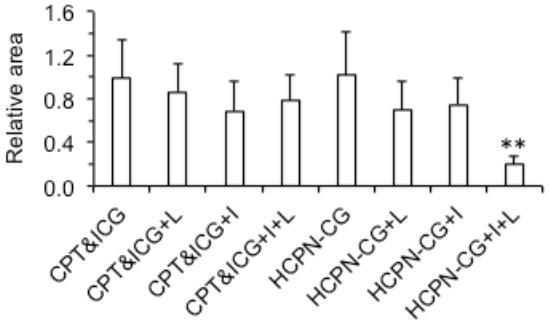

Figure S13. Quantitative data corresponding to the confocal images shown in Figure 4B. The data show the shrinkage of the 3D mammosphere cells treated with HCPN-CG nanoparticles, ice cooling (5 min), and laser irradiation (1 W/cm^2, 2 min) is significant. Error bars represent S.D. (n = 50). **: $p < 0.01$ (Kruskal-Wallis *H* test). I: ice and L: laser irradiation.

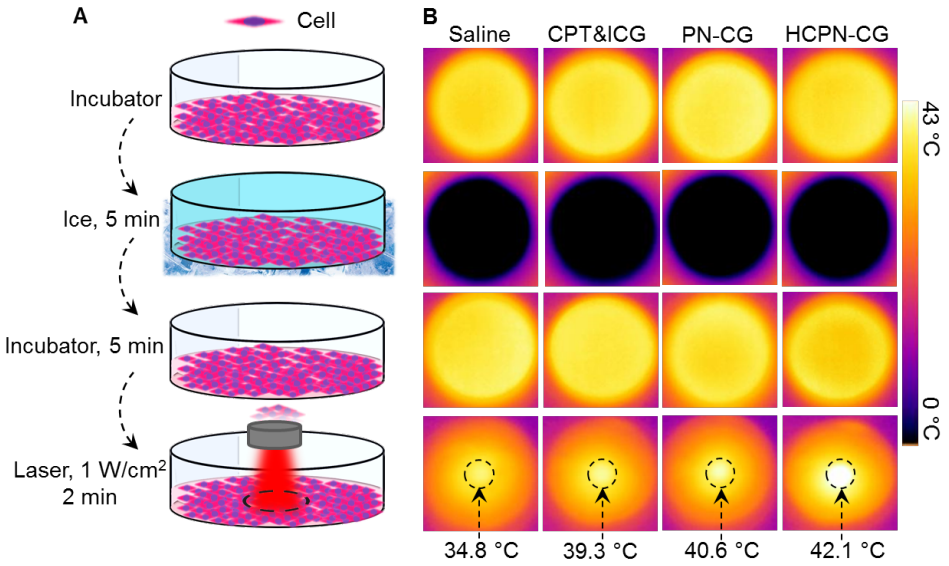

Figure S14. Infrared thermographic maps in 35 mm dish showing the temperature distribution during the treatment with ice cooling and laser irradiation. (A) A schematic illustration of the procedure for cell treatment in 35mm petri dish. (B) The thermographic images showing the temperature of cells with all the four treatment is ~37 °C in incubator, drops to 0-4 °C after incubated in ice for 5 min, and increase to ~37 °C when incubated in incubator for 5 min. After further irradiated with laser for 2 min at 1 W/cm^2: The temperature reached 34.8, 39.3, 40.6, and 42.1 °C for the saline, free CPT&ICG, PN-CG, and HCPN-CG treatments, respectively. All the drug formulations were replaced with fresh medium before ice cooling.

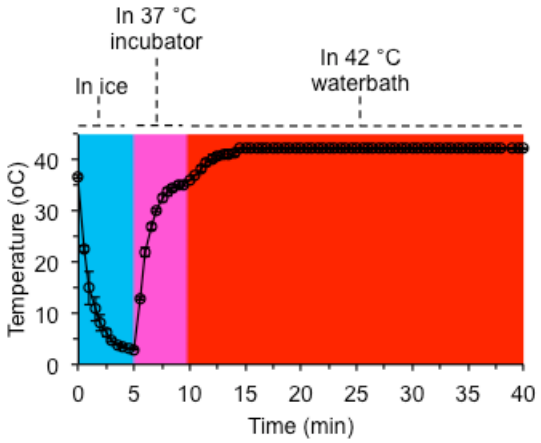

Figure S15. Thermal history of samples treated in ice (5 min), incubator (37 °C, 5 min), and waterbath (42 °C, 30 min).

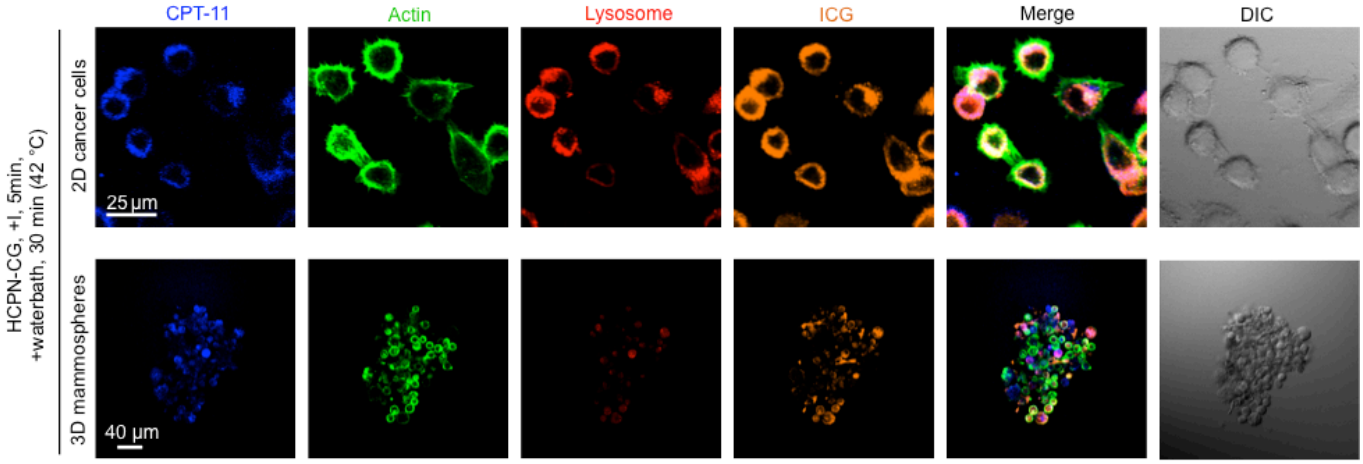

Figure S16. Impact of ice cooling and waterbath warming on 2D cancer cells and 3D mammospheres. Confocal images of 2D cancer cells and 3D mammospheres after incubated with HCPN-CG nanoparticles for 3 h at 37 °C, incubated in ice for 5 min, and warmed in waterbath (42 °C) for 30 min, showing waterbath warming induces less change in the cell morphology than laser heating although the maximum bulk temperature is all ~42 °C.

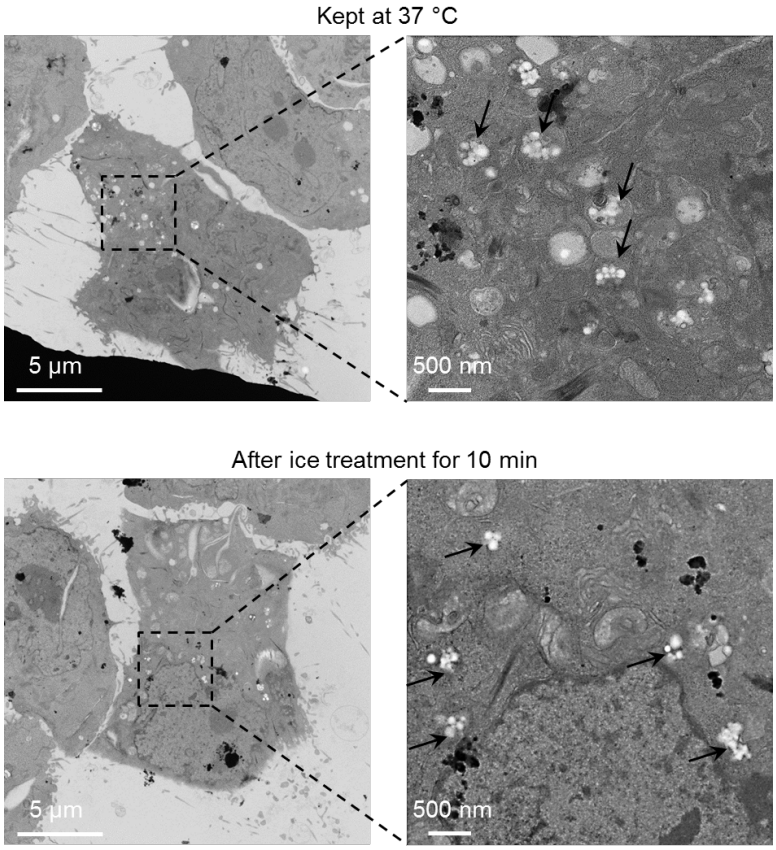

Figure S17. TEM images of cancer cells treated with nanoparticles synthesized by replacing PNIPAM-B with PLGA. Nanoparticles can be observed in cells kept at 37 °C or with ice cooling suggesting the nanoparticles are not cold-responsive inside cells, which is consistent with the data shown in Figure S5. Arrows indicate nanoparticles taken up in endo/lysosomes inside cells.

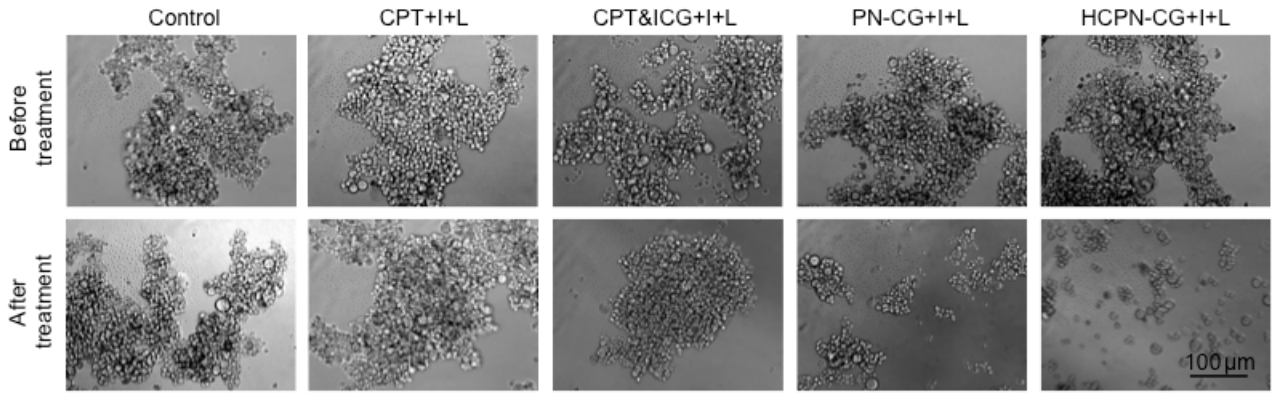

Figure S18. Typical micrographs showing morphology of the 3D mammospheres before (top row) and after (bottom row) treated with various drug formulations. I: ice cooling for 5 min and L: laser irradiation at 1 W/cm^2 for 2 min.

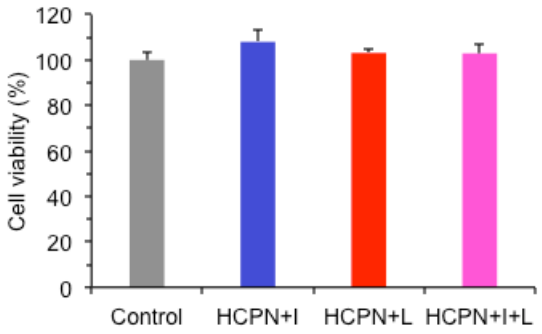

Figure S19. Cytotoxicity of blank HCPN nanoparticles in combination with ice (+I, 5 min), laser (+L, 1 W/cm^2, 2 min), or both (+I+L). The results indicate that blank HCPN nanoparticles are not harmful to cells even when combined with the ice and laser treatments.

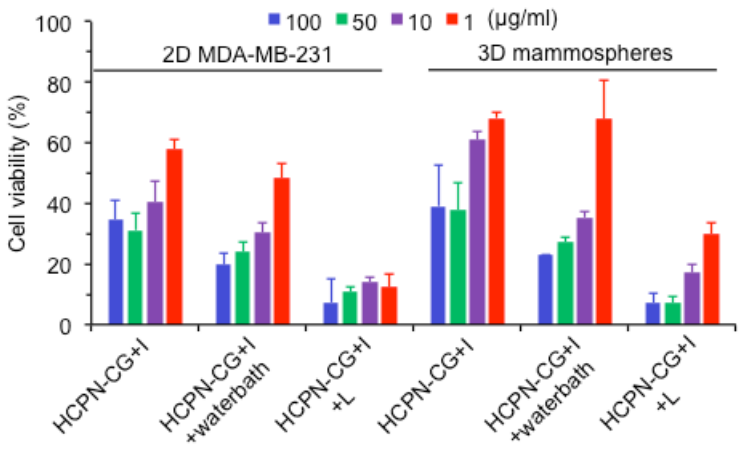

Figure S20. *In vitro* anticancer capacity of HCPN-CG nanoparticles with waterbath warming versus laser irradiation. Viability of 2D cancer cells and 3D mammosphere cells after treated with HCPN-CG nanoparticles for 12 h at 37 °C, followed by cooling on ice (HCPN+I, 5 min), cooling on ice (5 min) with waterbath (HCPN+I+waterbath, 30 min, 42 °C), and cooling on ice (5 min) with laser irradiation (HCPN+I+L, 1 W/cm^2, 2 min). The results show the waterbath warming is not as effective as laser irradiation in killing both the 2D cancer cells and the 3D mammospheres.

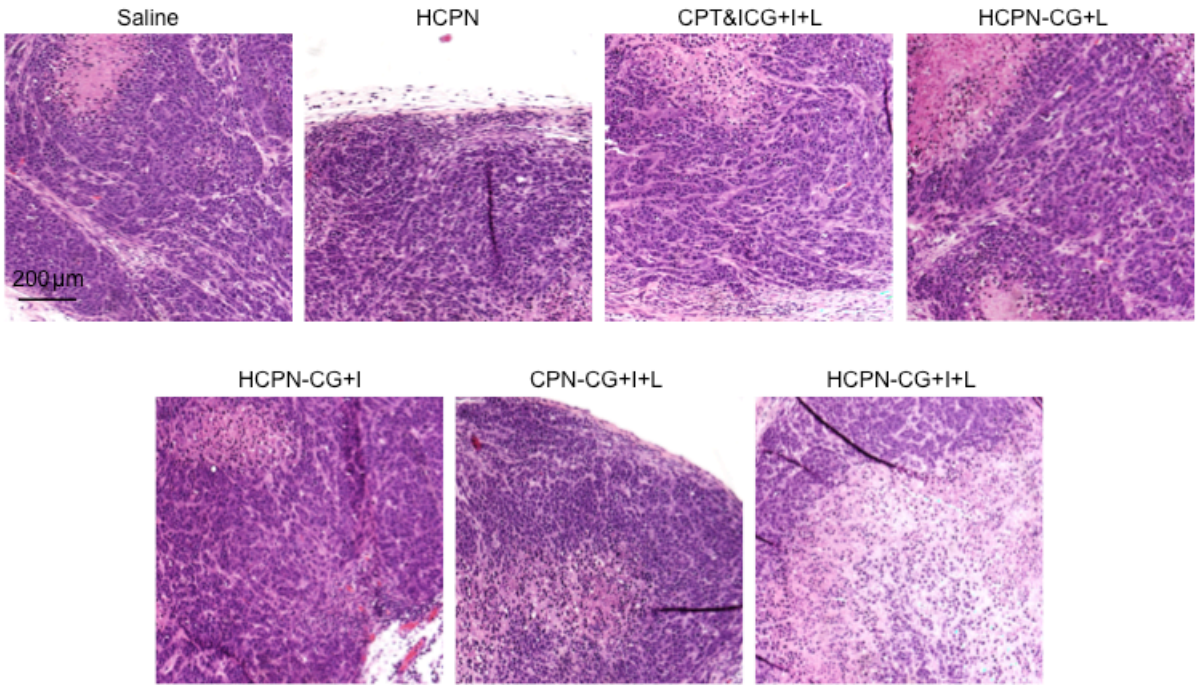

Figure S21. Representative histology images of the tumors with different treatments collected on day 30. The tissues were stained by hematoxylin and eosin (H&E). Extensive necrosis can be seen in the tumors from the HCPN-CG+I+L group while tumors from all the remaining groups appear more viable. I: ice cooling for 5 min and L: laser irradiation at 1 W/cm^2 for 2 min.

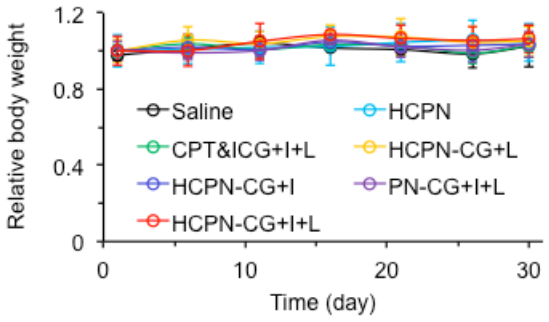

Figure S22. Relative (to saline control) body weight of the mice with the various treatments. The data show no significant difference between the different groups. Error bars represent ± S.D. (n = 5). I: ice cooling for 5 min and L: laser irradiation at 1 W/cm^2 for 2 min.

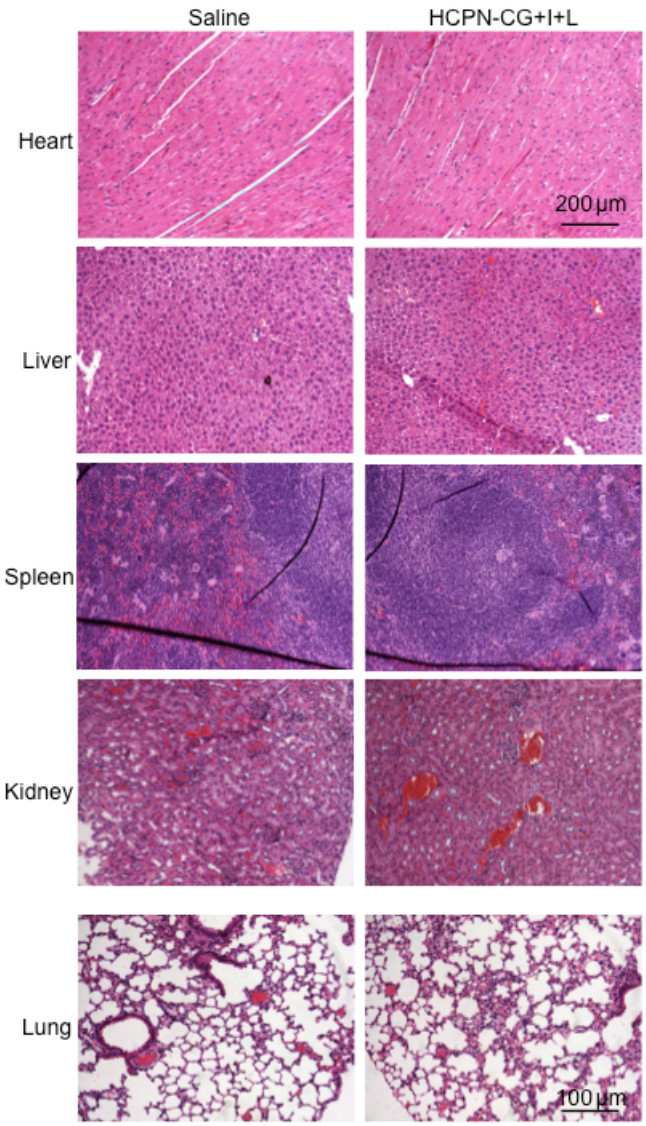

Figure S23. No evident toxicity to critical organs is observable for the HCPN-CG nanoparticles *in vivo*. Representative hematoxylin&eosin (H&E) stained tissue of five critical organs in mice with saline and HCPN-CG+I+L treatments. I: ice cooling for 5 min and L: laser irradiation at 1 W/cm^2 for 2 min.

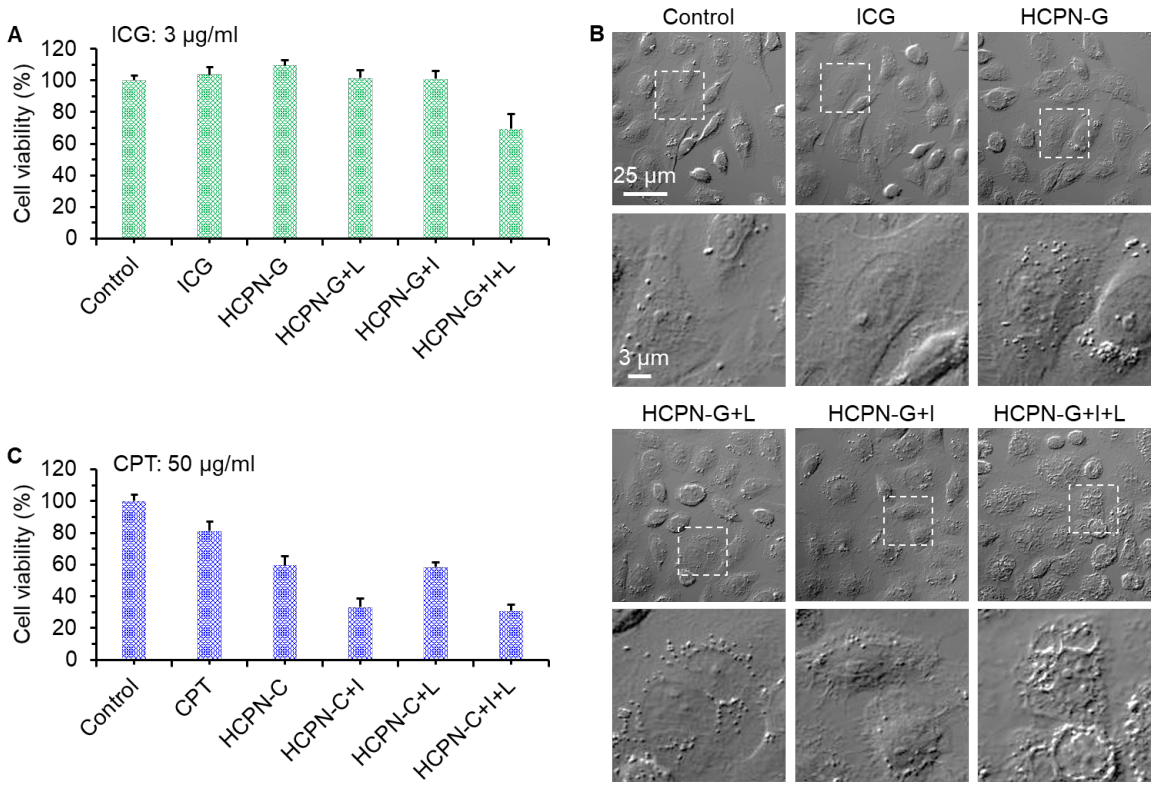

Figure S24. *In vitro* anticancer capacity of HCPN nanoparticles encapsulated with ICG (G) or CPT (C) alone with or without laser irradiation and/or ice cooling. (A) Viability of MDA-MB-231 cells and (B) photographs of the cells, showing that ICG is not cytotoxic even after encapsulated inside the HCPN nanoparticles (HCPN-G) with ice cooling or laser irradiation. When combined with both ice cooling and laser irradiation (HCPN-G+I+L), it can cause cytotoxicity because of the damage to the cell morphology as shown in (B). (C) CPT is toxic to cancer cells, which is further improved by encapsulating it inside the HCPN nanoparticles (HCPN-C). Ice cooling could enhance the cytotoxicity of HCPN-C probably via burst drug release while laser irradiation could not. The latter is because there is no photothermal warming in the absence of ICG.

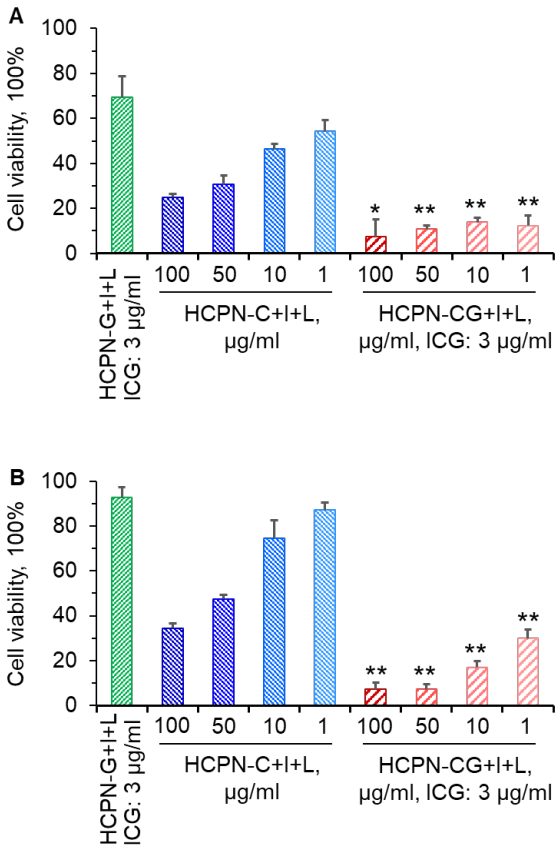

Figure S25. *In vitro* anticancer capacity of HCPN nanoparticles encapsulated with ICG (G) or CPT (C) of different concentrations after laser irradiation and ice cooling. Viability of (A) 2D cultured MDA-MB-231 cells and (B) 3D microscale tumors enriched with CSCs treated with HCPN-G (ICG: 3 μg/ml), HCPN-C (CPT: 100, 50, 10 and 1 μg/ml) and HCPN-CG (CPT: 100, 50, 10 and 1 μg/ml; ICG: 3 μg/ml for all conditions) with both laser irradiation and ice cooling. The results indicate that HCPN-CG+I+L could generate significantly higher toxicity then HCPN-C and HCPN-G for both 2D and 3D cultured cells at all the conditions, confirming the advantages of encapsulating both CPT and ICG into HCPN nanoparticles. *: $p < 0.05$, **: $p < 0.01$, which indicates cells treated with HCPN-CG+I+L is significantly lower than treatments with the same drug concentration of HCPN-C+I+L. Cells treated with HCPN-CG+I+L for all the concentrations are significantly lower than HCPN-G treatment ($p < 0.01$).